

# Optimal Design of Advanced Reflectivity Control Device for Solar Sails Considering Polarization Properties of Liquid Crystal

By Hirokazu ISHIDA,<sup>1)</sup> Toshihiro CHUJO,<sup>1)</sup> Osamu MORI,<sup>2)</sup> Junichiro KAWAGUCHI<sup>2)</sup>

<sup>1)</sup>Department of Aeronautics and Astronautics, The University of Tokyo, Tokyo, Japan

<sup>2)</sup>Institute of Space and Astronautical Science, JAXA, Sagami, Japan

(Received June 21st, 2017)

The Reflectivity Control Device (RCD) is the external momentum exchange device. The RCD can control the solar radiation pressure that the device obtains by changing the reflectivity. The device has a mirror on which polymer dispersed liquid crystal (PDLC) layer is attached. By changing the electric field in the PDLC layer, we can control the transmittance of the sunlight through the layer, by which we can control the reflectance of the device. The RCD is thin-film-shaped and mounted on the solar sail's membrane. We are currently developing a new type RCD named Advanced-RCD (A-RCD). While the conventional RCD reflects the sunlight vertically, the A-RCD reflects it obliquely. This oblique reflection can generate a torque perpendicular to the solar sail's membrane, for example. The essential thing in the designing the A-RCD is that the PDLC layer has polarization properties for the oblique light transmission. We must take into account this property in designing the A-RCD optimally, since the sunlight passes the PDLC layer obliquely in the A-RCD. In this research, we evaluated the polarization properties of the PDLC and then executed Monte Carlo simulation to optimize the reflection angle of the A-RCD.

**Key Words:** Advanced Reflectivity Control Device, Polarization Property, Solar Sail, Polymer Dispersed Liquid Crystal

## Nomenclature

$n$	: refractive index
$\mu$	: attenuation coefficient
$\gamma$	: angle of incident to device
$\theta$	: directional angle
$\phi$	: polarization angle
$\alpha$	: inclination angle of slope
$I$	: intensity of light
$r$	: energy reflectance
$a$	: energy attenuation

## Subscripts

$LC$	: liquid crystal
$o$	: ordinary light
$e$	: extraordinary light
$s$	: s-polarized light
$p$	: p-polarized light

## 1. Introduction

The reflectivity Control Device (RCD) is a novel attitude control device using the solar radiation pressure (SRP).<sup>1)</sup> This device is thin-film-shaped. The RCD reflects sunlight diffusively and specularly, when the device is ON and OFF states, respectively. By using this difference of reflectivity, we can control the SRP that the device obtains. This device is applied to the attitude control of solar sails by putting the two RCDs across the center of gravity of the solar sail, for example as shown in Fig. 1. Unlike internal momentum exchange devices which require fuel to unload the accumulated angular momentum, the RCD is a fuel-free device. Furthermore, unlike magnetorquer, the RCD is useful even in deep space explorations because the RCD does not rely on the terrestrial magnetism.

In the RCD, Polymer Dispersed Liquid Crystal (PDLC) layer

is put between two polyimide-film, one of which is aluminum-deposited as shown in Fig. 2. The PDLC layer consists of small size droplets filled with nematic liquid crystals (hereinafter simply referred to as "LC"), and the polymer which surrounds the droplets. The efficacy of the RCD was demonstrated by an actual space mission named "IKAROS" launched by Japan Aerospace Exploration Agency (JAXA).<sup>2)</sup> The major problem arose in the operation of "IKAROS" was the deformation of the solar sail membrane that caused acceleration torque perpendicular to the solar sail membrane. This disturbance is called the windmill effect.<sup>3)</sup> This windmill effect becomes a significant problem especially when the mission period is long. For example, JAXA is now planning solar sail mission toward Tro-

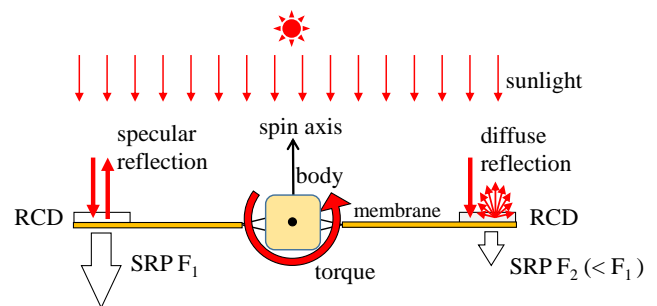


Fig. 1. Application of the conventional RCD to attitude control for solar sails.

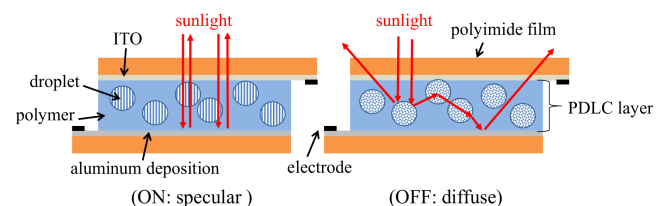


Fig. 2. Cross-sectional structure of the conventional RCD and the concept.

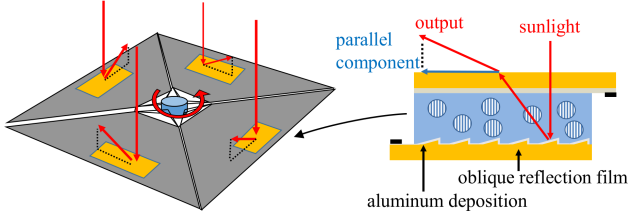


Fig. 3. Cross-sectional structure of A-RCD and how the devices generate torque. The parallel component of the outputted light contributes to the torque generation.

jan asteroid that takes 20 years.<sup>4)</sup> In this mission, we must use thruster requiring much fuel to counteract this effect over years.

As a solution to this problem, we are currently developing a new type RCD named Advanced-RCD (A-RCD) which reflects the sunlight obliquely instead of vertically.<sup>3)</sup> This device is useful not only for counteracting the windmill effect, but also for obtaining an additional degree of freedom of the attitude control. The sunlight reflected by the A-RCD has a component parallel to the membrane, which generates the torque perpendicular to the membrane. The cross-sectional structure of the A-RCD and how it works are shown in Fig. 3. The bottom polyimide has an aluminum deposited saw-tooth structure made by the polyimide film.

Obviously, there are oblique light transmissions through the layers in the A-RCD. The important thing here is that the PDLC layer in the A-RCD has the polarization properties for oblique light transmission. Also, each interface between the layers has the polarization properties due to Fresnel's law. Therefore, in order to maximize the transmittance (or the performance) of the A-RCD, it is necessary to take into account these polarization properties.

The A-RCD has many design parameters including reflection angle at the oblique reflection film, the thickness of layers, and the materials. Among these parameters, the reflection angle is the most important parameter because this parameter is related mostly to the polarization properties of the PDLC layer. Also, other parameters such as thicknesses and materials are pre-determined in most cases, because these parameters are restricted to the manufacturing process and the resistance to the space environment. In this context, we will discuss the optimization of the reflection angle in this paper.

We begin in Section 2 with a description of polarization properties of the PDLC layer. In Section 3, the experimental method to evaluate the polarization properties of the PDLC layer is introduced. The same section includes the results of the experiment. By using the experimental results, we will execute Monte Carlo simulation to optimize the reflection angle in Section 4.

## 2. Attenuation and polarization of light in the PDLC layer

### 2.1. Refractive indicatrix of LC

Before explaining the polarization properties of the PDLC, this section introduces the refractive indicatrix of the LC. The LC molecules are rod-like uniaxial shape, and hence can be considered to have axial symmetry as shown in Fig. 4. The axis is called *optic axis*, in general. Now we define the directional angle  $\theta$  as an angle between the optic axis and propagation direction of the light  $S$ ,  $\phi$  as an angle between the polarization

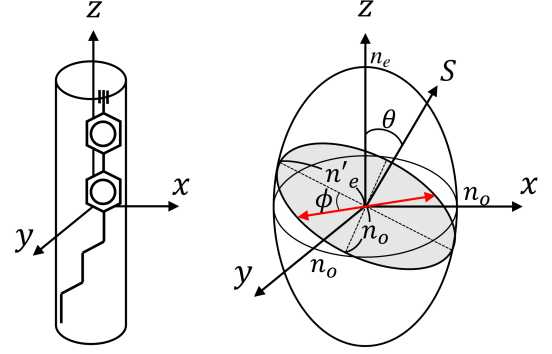


Fig. 4. Typical shape of LC molecules (left) and the refractive indicatrix (right) which corresponds to each other. The Z axes in both figures are identical with the optic axis.

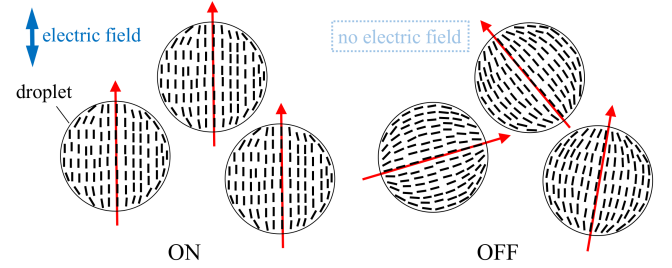


Fig. 5. ON and OFF states of LC molecule's alignment in the droplets. The red arrows indicate the orientations of the droplets.

plane and the plane spanned by  $S$  and optic axis. The refractive index  $n_{LC}$  of the LC molecule is then calculated as a function of  $\theta$  and  $\phi$  as follows,

$$n_{LC}(\theta, \phi) = \sqrt{\frac{n_o^2 n_e'^2(\theta)}{n_o^2 \sin^2 \phi + n_e'^2(\theta) \cos^2 \phi}}, \quad (1)$$

where,

$$n_e'(\theta) = \sqrt{\frac{n_o^2 n_e^2}{n_o^2 \sin^2 \theta + n_e^2 \cos^2 \theta}}. \quad (2)$$

$n_{LC}$  equals to  $n_o$  for ordinary light ( $\theta = 0$ ), and equals to  $n_e$  for extraordinary light ( $\theta = \pi/2, \phi = 0$ ). The refractive index  $n_e$  of typical LCs is 0.1 to 0.2 greater than  $n_o$ . The dependency of  $n_e'$  on  $\theta$  and  $\phi$  is concisely described by the diagram called refractive indicatrix as shown in Fig. 4, and  $n_{LC}$  is calculated using this diagram as follows. First, cut the ellipsoid to obtain the ellipse with major axis  $n_e'(\theta)$  and minor axis  $n_o$ . Second, obtain the line of intersection of the ellipse and polarization plane. Then, the half of the distance of this intersection line indicates  $n_{LC}$ . Now, let us consider two different polarized light: (a) light with  $\phi = 0$ , (b) light with  $\phi = \pi/2$ . When the light (a) passes through the LC molecule, the  $n_{LC}$  equals to  $n_o$  regardless of  $\theta$  because the minor axis of the cross-sectional ellipse is always  $n_o$ . In the case for the light (b), however, the  $n_{LC}$  varies from  $n_o$  to  $n_e$  as  $\theta$  increases from 0 to  $\pi/2$ . This is because the major axis of the cross-sectional ellipse varies from  $n_o$  to  $n_e$  depending on  $\theta$ .

### 2.2. Polarization properties of PDLC layer

As briefly introduced in Section 1, the PDLC layer is composed of droplets filled with LC molecules and polymer that surrounds the droplets. The light attenuation in a medium is mainly caused by the scattering and absorption. For the PDLC

case, the former one is dominant because both the polymer and LC are transparent media. In the PDLC, light scattering is caused by the mismatches of refractive indices between the polymer and droplet, which makes the medium inhomogeneous. The typical PDLC is designed such that refractive index  $n_p$  of polymer is the same as  $n_o$ .

When an electric field is applied in the PDLC layer, the LC molecules in droplets align along the direction of the electric field as shown in Fig. 5. The illustration also shows that some LC molecules are anchored to the droplet wall, and hence the LC molecules are not completely aligned. However, in an approximate manner, all LC molecules can be considered to align along the electric field.<sup>5)</sup> On this approximation, the refractive index of the droplet equals to  $n_o$  for any vertical incident light ( $\theta = 0$ ), and hence there is no mismatch of  $n_p$  and  $n_{LC} = n_o$ . Therefore, the vertically incident light is hardly be scattered in the PDLC in the ON-state. On the other hand, when an electric field is not applied, the LC-director field in the droplets and the orientation of the droplets are not uniform as illustrated in Fig. 5. These random orientations cause the light scattering because the light propagating in any direction experiences the mismatches of the refractive index between the polymer and droplets. This difference of scattering properties is the reason why the PDLCs are used as light valves.

For the obliquely incident light, the scattering properties of the PDLC depends on both the directional angle  $\theta$  and the polarization angle  $\phi$ . Now, Let us consider the two oblique incidents: (A) an incident light with  $\phi = 0$ , (B) an incident light with  $\phi = \pi/2$ . The former and the latter respectively correspond to the case for light (a) and light (b) in the previous subsection. For case (A), from the explanation in the previous subsection,  $n_{LC}$  varies from  $n_o$  to  $n_e$  as  $\theta$  changes from 0 to  $\pi/2$ . Therefore, the light with  $\phi = 0$  incurs the higher degree of scattering as  $\theta$  increases. On the other hand, for case (B),  $n_{LC}$  takes a constant value  $n_o$ , and hence the degree of scattering of case (B) is constant. Case (A) and (B) are the extreme situations, and the degree of scattering of the PDLC for any polarization has a property between case (A) and (B).

From the discussion above, we can expect that the PDLC layer works as a *polarizer* especially for the case of large  $\theta$ , in the sense that the light with  $\phi = 0$  attenuates in the PDLC more than the light with  $\phi = \pi/2$ .

### 3. Experimental method to obtain attenuation coefficient

#### 3.1. Attenuation coefficient

In this paper, we refer to energy attenuation and energy reflectance as simply “attenuation” and “reflectance”. The attenuation of the light beam in the PDLC layer is well described by the exponential decrease of the light intensity.<sup>6)</sup> We introduce attenuation coefficient  $\mu$ , which is defined as follows

$$\mu = -\frac{1}{x} \ln \left( \frac{I(x)}{I_0} \right) \quad (3)$$

where  $x$  is the passing distance of the light,  $I_0$  and  $I(x)$  are the incident and transmitted intensity (energy per unit area), respectively. The validity of the Eq. 3 is limited to the case when the contribution of scattered light is small compared to the direct attenuated beam.<sup>6)</sup> In this paper, we assume that the contribution

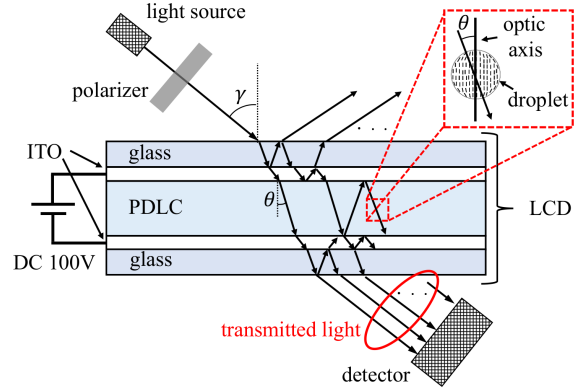


Fig. 6. Experimental setup and internal multiple reflection. Note that the size of the LCD is exaggerated in this image.

of scattered light is negligible. From the discussion in Section 2, the attenuation in the PDLC layer depends on the both the directional angle  $\theta$  and polarization angle  $\phi$ . To investigate dependency of  $\mu$  on  $\phi$  and  $\theta$ , considering the two cases  $\phi = 0$  and  $\phi = \pi/2$  is enough. This is because any polarization can be represented in terms of 2 orthogonal polarized components. In the following subsections, we introduce the experimental method to obtain the dependency of  $\mu$  on  $\phi$  and  $\theta$ , and then show the experimental results.

#### 3.2. Experimental method

The attenuation coefficients of PDLC is measured using a spectrometer and the prepared liquid crystal device (LCD). The LCD is composed of ITO deposited glass and 20  $\mu\text{m}$  thick PDLC layer as shown in Fig. 6. The spectrometer emits the light varying the wavelength and detects the transmitted light through the LCD. In the PDLC layer, we applied the voltage of DC 100 V to keep the device ON-state. A polarizer is put just after the light source of the spectrometer. By rotating the polarizer, we can obtain light source that has polarization angle  $\phi = 0$  and  $\phi = \pi/2$ . The light with  $\phi = 0$  and the light with  $\phi = \pi/2$  have the polarization planes parallel and perpendicular to the incident plane, respectively, and hence hereinafter we refer to these two polarized lights as s- (senkrecht-) and p- (parallel-) polarized light. The LCD is held on a stand that can change  $\gamma$  between 0 and 70 deg.

Using this experimental setup, we can obtain  $\mu_{LC}$  for s- and p- polarized light and for the different incident angle and wavelength. Since the LCD has 5 layers (glass-ITO-PDLC-ITO-glass) that have different refractive indexes, there occurs multiple reflections at each interface as illustrated in Fig. 6. Therefore, the detector of the spectrometer detects the sum of the multiple-reflected light as a global transmission. We have to take into account the multiple reflections to calculate  $\mu$ .

When the reflectance at each interface and absorption in each layer are known, it is possible to calculate transmittance in a probabilistic way. The multiple reflections at the layers are expressed as the probability transition diagram shown in Fig. 7. When the multilayer specimen is composed of  $n - 1$  layers, the system has  $2n + 1$  states. States  $s_1$ ,  $s_2$ , and  $s_{2n+1}$  indicate the energy of whole incident light, global reflection, and global transmission, respectively. Let us consider the layer  $k$  with an attenuation rate  $a_k$ . Also let us consider the interfaces  $k$  and  $k + 1$  with reflectance rates  $r_k$  and  $r_{k+1}$ , respectively. These two

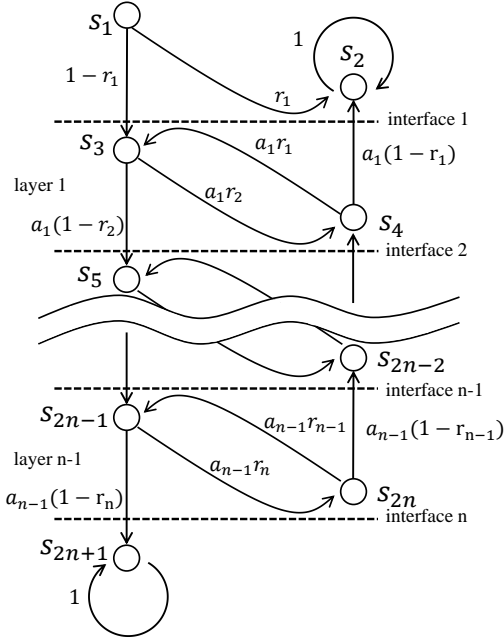


Fig. 7. Probability transition diagram for a specimen with  $n - 1$  layers. Each node and arrow represents a state of the light and transition probability, respectively.

interfaces sandwich the layer  $k$ . In the layer  $k$ ,  $s_{2k+1}$  and  $s_{2k+2}$  are the states of light which go forward and backward direction, respectively. The transition probability  $\Pr(s_{2k+1} \rightarrow s_{2k+2})$  equals to  $a_k r_k$  because the light attenuates with rate  $a_k$  to reach the interface  $k$  and then reflected there with a reflectance rate  $r_{k+1}$ .  $\Pr(s_{2k+1} \rightarrow s_{2k+3})$  equals to  $a_k(1 - r_{k+1})$ , and  $1 - r_{k+1}$  is the transmission probability at the interface  $k + 1$ . Similarly,  $\Pr(s_{2k+2} \rightarrow s_{2k+1}) = a_k r_k$  and  $\Pr(s_{2k+2} \rightarrow s_{2k}) = a_k(1 - r_k)$ . As shown in Fig. 7,  $s_2$  and  $s_{2n+1}$  transfer themselves with probability 1. The  $2n + 1 \times 2n + 1$  transfer matrix corresponding to the diagram in Fig. 7 is defined as  $M$ , and  $2n + 1$  dimensional initial state vector is defined as  $s_0 = [1, \mathbf{0}_{1 \times 12}]^T$ . The steady state vector  $s_\infty$  is calculated as follows,

$$s_\infty = M^\infty s_0. \quad (4)$$

The  $2n + 1$ -th element of  $s_\infty$  corresponds to the global transmittance of the device. A similar calculation technique is proposed in Ref. 7).

As for the LCD in this experiment, we neglected the attenuation at the glass layers because its attenuation coefficient is second orders of magnitude less than the attenuation coefficient of PDLC layer. Also, we considered the attenuation in the ITO layer as negligible because the ITO was deposited with nanometer scale. We can calculate the reflectance rate for s- and p-polarized light by using Fresnel's equation as follows,

$$r_s = \left[ \frac{n_b \cos \alpha - n_a \cos \beta}{n_b \cos \alpha + n_a \cos \beta} \right]^2 \quad (5)$$

$$r_p = \left[ \frac{n_a \cos \alpha - n_b \cos \beta}{n_a \cos \alpha + n_b \cos \beta} \right]^2 \quad (6)$$

where  $n_a$  and  $n_b$  are the refractive index of the medium of the incident- and refractive- sides, respectively.  $\alpha$  and  $\beta$  are the angle of incident and angle of refraction, respectively. When  $\gamma$  is given, we can calculate the angles of incident and refraction in

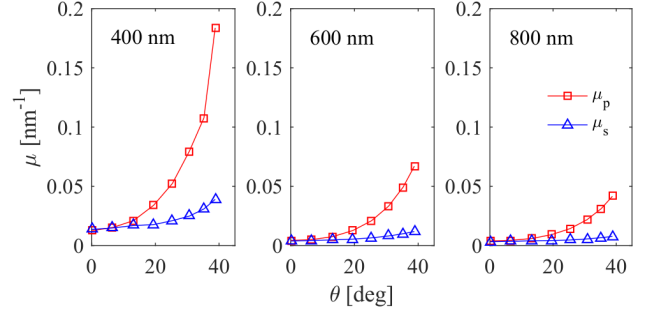


Fig. 8. Attenuation coefficient PDLC layer for s- and p-polarized light.

all layer by using Snell's law. In the following calculations, we set refractive index of glass to 1.51, which equals to soda-lime glass that we used in the LCD. The refractive index of PDLC layer is set to the refractive index  $n_p$  of the polymer because the polymer, not droplets, contacts the other layers.  $n_p$  is set to 1.5 which is a common value for  $n_p$ . We referred to Ref. 8) to set the refractive index of ITO for each wavelength. In this problem,  $M$  is a  $13 \times 13$  matrix, and the matrix is a function of a single variable  $a_{LC}$  (attenuation rate in PDLC layer). We can obtain  $a_{LC}$  by solving the following equation for  $a_{LC}$ :

$$e_{13} M^\infty s_0 = T \quad (7)$$

where  $e_{13} = [\mathbf{0}_{1 \times 12}, 1]^T$ , and  $T$  is the global transmittance that spectrometer detects. Then  $\mu$  is calculated as follows.

$$\mu = -\frac{\ln(a_{LC}) \cos \theta}{d} \quad (8)$$

where  $d$  is the thickness of the PDLC layer,  $\theta$  is the angle between the direction of the light and normal vector of the LCD surface, and also identical to  $\theta$  in Section 2.

### 3.3. Results

We conducted the experiment and analysis described in the previous subsection. The wavelength was changed in the range between 400nm and 800nm at an incremental width of 10 nm. The incident angle  $\gamma$  was changed in  $0 \leq \gamma \leq 70$  deg (corresponding to  $0 \leq \theta \leq 38.8$  deg) at an incremental width of 10 deg.

Fig. 8 shows the experimental results. As discussed in Section 2,  $\mu_p$  shows the steep increases as  $\theta$  increases. Also,  $\mu_s$  takes almost constant value. The slight increase of  $\mu_s$  is considered to be caused by the curvilinear alignment of LC molecules in the droplets described in the . From this result, the PDLC has polarization properties especially when  $\theta$  is large in the sense that  $\mu_p$  is greater than  $\mu_s$ .

## 4. Optimal design of reflection angle

### 4.1. Monte Carlo simulation

The performance of the A-RCD is defined by the parallel component of the momentum of the outputted light. In a strict sense, the scattered light, as well as the direct light beam, contributes to the performance. However, in this paper, we assume that the contribution of scattered light is negligible, for simplicity. To obtain the relationship between the performance of the A-RCD and reflection angle of the oblique reflection film, we performed Monte Carlo simulation. By this stochastic approach, we can take into account the energy reflectance at each

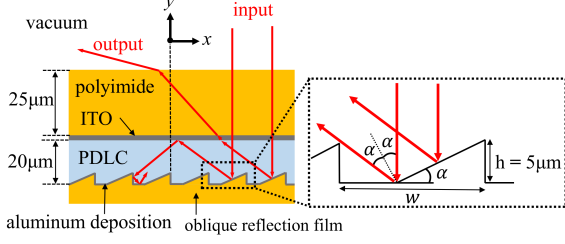


Fig. 9. Cross-sectional view of the parts of the periodic structure of the A-RCD.

layer calculated by Eq. (5) and Eq. (6), as well as energy attenuation in each layer. Fig. 9 shows the A-RCD model used in the simulation. The oblique reflection film has a saw-tooth pattern with tiny flat parts between cycles. The flat parts prevent the primary reflected light at the slope from reflecting at the vertical part toward counter direction against the requirement. When we fix the height  $h$  of the saw-tooth structure, the shape of the reflection layer is uniquely determined only by the slope inclination angle  $\alpha$ . The cycle width  $w$  is defined in Fig. 9. Note that this simulation was performed in a two dimensional space because the cross-sectional structure in Fig. 9 of the A-RCD is the same in the direction perpendicular to the paper.

The attenuation coefficient of the PDLC set to the values obtained by the experiment in Section 3.  $\mu$  for any directional angle  $\theta$  is gained by applying spline-interpolation ( $0 \leq \theta \leq 38.8$  deg) and linear extrapolation ( $\theta > 38.8$  deg) to the experimental data. The extrapolation is obtained using data of  $\theta = 60, 70$  deg. The attenuation coefficient and refractive index of polyimide (APICAL-AH) are obtained by using a spectrophotometer and spectroscopic ellipsometer. The refractive index of ITO for particular wavelength are the same as values used in Section 3. We considered that aluminum deposition on the saw-tooth structure perfectly reflects the sunlight.

Hereinafter, we refer to the light for each Monte Carlo trial as a photon. Each photon has an energy of  $E = 1$  with the propagation vector  $\mathbf{u} = [0, -1]^T$  at the initial state. The initial  $x$  of the photons are determined by the uniform random number between 0 and  $w$  considering the periodicity of the saw-tooth pattern. These initial conditions are equivalent to the uniform vertical incident of light to the whole area of the A-RCD. Since the sunlight, which is an unpolarized light, can be decomposed into two orthogonal polarizations, performing the simulations for the s- and p-polarized light for the same number of trials is sufficient. In this simulation, s- and p- polarized light is defined with reference to the incident plane spanned by  $\mathbf{u}$  of inputted light and  $\mathbf{u}$  of outputted light. We performed  $N = 10000$  times trials for both s- and p- polarized light, which sums up to  $2N$  times trials.

When each outputted photon has an energy  $E'$  with the propagation vector  $\mathbf{u}'$ , the performance of the A-RCD  $p$  for a light with wavelength  $\lambda$  can be evaluated in a dimensionless manner as follows,

$$p(\lambda) = \frac{1}{2N} \sum_{j=1}^{2N} E'_j \mathbf{e}_2 \mathbf{u}'_j \quad (9)$$

where  $\mathbf{e}_2 = [0, 1]^T$ . Now, since the A-RCD is used in the space, the performance of the A-RCD taking into account the solar

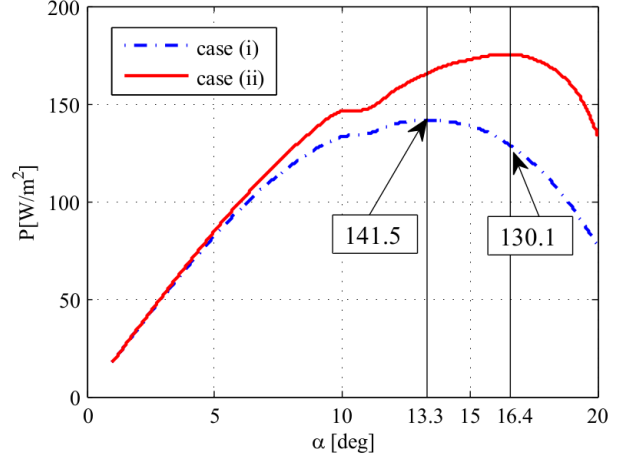


Fig. 10. The dependency of  $P$  on inclination angle  $\alpha$ .

spectrum<sup>9)</sup>  $S(\lambda)$  can be calculated as follows,

$$P = \int_{\lambda_1}^{\lambda_2} p(\lambda) S(\lambda) d\lambda. \quad (10)$$

For this purpose, we performed Monte Carlo simulation above changing the wavelength. For simplicity, the wavelength was changed in the visible light range ( $\lambda_1 = 400$  nm and  $\lambda_2 = 800$  nm) at an incremental width of 10 nm.

#### 4.2. Simulation result

We executed the Monte Carlo simulation above for the following two cases: (i) considering the polarization properties of the PDLC, (ii) not considering the polarization properties of the PLDC. In case (i), we used  $\mu$  depending on  $\theta$  obtained in the experimental results. In case (ii), we used the  $\mu$  against the light with  $\theta = 0$  regardless of the actual  $\theta$ . Case 2 occurs when the designer does not know the angular dependency of  $\mu$  of the PDLC. Fig. 10 shows the dependency of the performance  $P$  of the A-RCD on the slope inclination angle  $\alpha$ . The red line and blue line plot the results of case (i) and (ii), respectively. Fig. 10 shows the gradually increasing the gap between the angular dependent performance curve for case (i) and (ii). This tendency can be easily explained by the experimental result that the  $\mu_p$  increases steeply as  $\theta$  increase. In this case,  $\theta$  equals to  $2\alpha$ . According to Fig. 10, the optimal  $\alpha$  for cases (i) and (ii) are 16.4 deg and 13.3 deg, respectively. This difference of the optimal angle is easily explained by the angular dependency of  $\mu_p$ . The optimized performance in case (i) is 141.5 W/m<sup>2</sup>. The performance calculated in case (i) using the optimized angle in case (ii) is 130.1 W/m<sup>2</sup>. From these results, the optimized performance considering polarization properties of the PDLC is 8.8% greater than the optimized result without consideration of the polarization properties.

#### 5. Conclusion

We performed the experiments and analysis to evaluate the polarization properties of PDLC layer by obtaining attenuation coefficient  $\mu$  of the PDLC layer. The experimental results show that while  $\mu_s$  takes an almost constant value,  $\mu_p$  becomes greater as  $\theta$  increases. This result indicates the polarization properties of PDLC layer especially when  $\theta$  is large, in the sense that  $\mu_p$  is greater than  $\mu_s$ . By using this result, we executed Monte

Carlo simulation to optimize the slope inclination angle  $\alpha$  of oblique reflection film of the A-RCD. Also, we performed the same simulation without considering the polarization properties of the PDLC layer. The two simulations show that the performance curves depending on  $\alpha$  are substantially different from each other. Moreover, the optimized performance considering polarization properties of the PDLC is 8.8% greater than the optimized result without consideration of these properties. From these results, we can conclude that polarization properties of the PDLC are not negligible in designing the A-RCD.

### Acknowledgments

I am grateful to T. Akiba, H. Yokota and K. Isoda from Tokyo Metropolitan Industrial Technology Research Institute for measuring the optical properties of the polyimide film.

### References

- 1) Funase, R., Shirasawa, Y., Mori, O., Tsuda, Y., Saiki, T., and Kawaguchi, J.: On-orbit verification of fuel-free attitude control system for spinning solar sail utilizing solar radiation pressure, *Advances in Space Research.*, **48**(2011), pp. 1740–1746.
- 2) Tsuda, Y., Mori, O., Funase, R., Sawada, H., Yamamoto, Takayuki., Saiki, Takanao., Endo, Tatsuya., Tonekura, Katsuhide, Y., Hoshino, H., and Kawaguchi, J.: Achievement of IKAROS-space solar sail demonstration mission, *Acta Astronautica.*, **82.2**(2013), pp. 183-188.
- 3) Chujo, T., Shirasawa, Y., Mori, O., and Kawaguchi, J.: Study and Development of Advanced Reflectivity Control Device for Spin Rate Control, 30th International Symposium on Space Technology and Science, Kobe, Hyogo, 2015.
- 4) Matsumoto, J., Funase, R., Mori, Osamu., Shirasawa, Y., Ono, G., Hamasaki, T., Hayashi, N., Chujo, T., Motooka, N., Tanaka., K.: Mission Analysis of Sample Return from Jovian Trojan Asteroid by Solar Power Sail, *Trans. JSASS Aerospace Tech. Japan*, **12**, ists29 (2014), pp.Pk\_43–Pk\_50.
- 5) Wu, B. G., West, J. L., and Doane, J. W.: Angular discrimination of light transmission through polymer-dispersed liquid-crystal films, *Journal of applied physics*, **62.9**(1987), pp. 3925–3931.
- 6) Zumer, S., Golemme, A., and Dane, J. W.: Light Extinction in a dispersion of small nematic droplets, *JOSA A*, **6.3**(1989), pp. 433–411.
- 7) Hebert, M., Hersch, R. D., and Becker, J. M.: Compositional reflectance and transmittance model for multilayer specimens, *JOSA A*, **24.9**(2007), pp. 2628-2644.
- 8) Moerland, R. J., and Hoogenboom, J. P.: Subnanometer-accuracy optical distance ruler based in fluorescence quenching by transparent conductors: supplementary material. *Optica*, **3.2**(2016), pp. 112-117.
- 9) Air Mass Zero Spectra, American Society for Testing and Materials, <http://rredc.nrel.gov/solar/spectra/am0/ASTM2000.html> (accessed March 30 2017)